Many-body electronic structure calculations of Eu-doped ZnO

M. Lorke* and T. Frauenheim
Bremen Center for Computational Materials Science, University of Bremen, Am Fallturm 1, 28359 Bremen, Germany

A. L. da Rosa
Universidade Federal de Minas Gerais, Dept. of Physics, Av. Antônio Carlos, 6627, 31270-901 Belo Horizonte, MG, Brazil
(Received 29 January 2015; revised manuscript received 23 February 2016; published 18 March 2016)

The formation energies and electronic structure of europium-doped zinc oxide has been determined using DFT and many-body GW methods. In the absence of intrisic defects, we find that the europium-f states are located in the ZnO band gap with europium possessing a formal charge of 2+. On the other hand, the presence of intrinsic defects in ZnO allows intraband f-f transitions otherwise forbidden in atomic europium. This result corroborates with recently observed photoluminescence in the visible red region S. Geburt *et al.* [Nano Lett. **14**, 4523 (2014)].

DOI: 10.1103/PhysRevB.93.115132

I. INTRODUCTION

Doping has been widely used to tailor the electronic, magnetic, and optical properties of semiconductors. Wide band-gap semiconductors such as ZnO are attractive for ultraviolet light-emitting diodes, lasers and high-power photonic applications. In ZnO, rare-earth elements can be incorporated in the material and the long lifetimes of the excited states allow for an easy realization of population inversion with promising applications in optoelectronic applications [1–5]. ZnO has a large band gap of 3.4 eV and a high thermal conductivity, enabling new electroluminescent devices.

Channeling experiments [6,7] indicate, that rare-earth elements in ZnO are preferentially incorporated at cation sites. More recent photoluminescence (PL) and photoluminescence excitation (PLE) investigations on ZnO nanoparticles corroborate this finding [8,9]. PL investigations of Eu-doped ZnO nanoneedles showed sharp emission lines from Eu^{3+}, suggesting the emission arises from intra-4f transitions, in addition to the ZnO interband emission [10]. The f-to-f transitions are forbidden in the isolated atom. However, the spherical symmetry is broken when the impurity is incorporated into the ZnO matrix. Besides Eu, optical emission from rare-earth orbitals has been achieved in ZnO nanowires implanted with erbium and ytterbium [5] and thin ZnO films doped with erbium, samarium, and europium [11–14]. The above experimental investigations have suggested explanations for the optical activation of rare-earths in ZnO [15,16] by means of substitutional hydrogen incorporation [15] or formation of defect complexes [8,16,17].

Theoretical investigations using density functional theory (DFT) in the generalized-gradient approximation (GGA) have performed for Eu doped ZnO [18,19], but were unable to ascertain the origin of the experimentally observed emission in ZnO. The main challenge here is the correct description of both ZnO band edges and defect states. It is common understanding that the use of local exchange-correlation functionals wrongly described the ZnO band gap, which could lead to misleading conclusions on the location of the impurity rare-earth f states. It has been shown that the correct description of the band gap is of paramount importance for the understanding of impurity and defect states in semiconductors [20–24]. Besides, intrinsic defects may also play an important role, since during ion implantation they are often introduced in ZnO. Jiang *et al.* [25] have shown that for many open d- or f-shell compounds the GW approach can provide a consistent and accurate treatment for both localized and itinerant states.

Using DFT calculations and the GW technique, we have previously shown that a complex containing a single oxygen interstitial defect and an europium atom substituting a zinc atom is a probable candidate to explain the observed emission in the red region of the spectrum in europium-doped ZnO nanowires [1]. Note that GW calculations do not include excitonic electron-hole interactions.

In this work, we show GW_0 calculations, as implemented in VASP, for Eu doped ZnO. Besides the work reported in Ref. [1], we have considered the presence of the most common defects in ZnO, such as oxygen and zinc vacancies and interstitials. The wave functions are kept fixed to the GGA level, whereas the eigenvalues are updated in the Green's function only. Here we show that this kind of defect has a relatively low formation energy and suggest possible mechanisms for the formation of such defect. Besides, we investigate other defects and calculate their formation energies and electronic structure.

II. COMPUTATIONAL DETAILS

In this work, we have employed density functional theory (DFT) [26,27] and many-body GW techniques [28] to investigate the formation energies and electronic structure of Eu-doped ZnO. The projected augmented wave method (PAW) [29] has been used as implemented in the Vienna *ab initio* package (VASP) [30,31]. A $3 \times 3 \times 2$ supercell containing 72 atoms with a $(2 \times 2 \times 1)$ **k**-point sampling and a cutoff of 500 eV is used to calculate all isolated intrinsic defects and complexes. For Eu_2O_3, we have used $(2 \times 2 \times 2)$ k points. For Eu metal, we adopted a bcc structure with a $(6 \times 6 \times 6)$ **k**-point mesh.

*mlorke@uni-bremen.de

A. Thermodynamic properties

To verify the thermodynamic stability of the investigated defect complexes, we follow the approach derived by van de Walle and Neugebauer [32]. The formation energy of a neutral defect or impurity is defined as

$$E_{\mathrm{f}} = E_{\mathrm{tot}}^{\mathrm{ZnO-defect}} - E_{\mathrm{tot}}^{\mathrm{ZnO-bulk}} - \sum_i n_i \mu_i + \mathrm{q}(\mathrm{E_v} - \mathrm{E_F}), \tag{1}$$

where $\mathrm{E_{tot}}$(ZnO-defect) is the total energy of a defective supercell and $\mathrm{E_{tot}}$ ZnO-bulk is the total energy for the supercell of pure ZnO. n_i is the number of atoms of type i (defects or impurities) that have been added to or removed from the supercell and μ_i is the corresponding chemical potential of each species, q is the charge of the defect. The Fermi level E_F is referenced with respect to the valence band maximum E_v of the host.

The lower bound of the chemical potential corresponds to the total absence of impurities/defects in the material. An upper bound on the chemical potential is given by the energy of the elemental bulk phase or other solubility-limiting phases. Formation of Eu clusters (metal) can be avoided by imposing the europium chemical potential to obey to

$$\mu_{\mathrm{Eu}} \leqslant \mu_{\mathrm{Eu(Eu\text{-}bulk)}}, \tag{2}$$

where Eu-bulk is the total energy of europium bulk in a bcc structure. Formation of europium precipitates are avoided by considering the bound for Eu_2O_3, a very stable phase of europium:

$$\mu_{\mathrm{Eu}} \leqslant \mu_{\mathrm{Eu(Eu_2O_3)}}. \tag{3}$$

The oxygen and zinc chemical potentials are not independent, but related by $\mu_{\mathrm{ZnO}} = \mu_{\mathrm{Zn}} + \mu_O$, where μ_{Zn}, μ_O and μ_{ZnO} are the zinc, oxygen, and zinc oxide chemical potentials, respectively. ΔH^{ZnO} is the formation enthalpy of ZnO. Combining Eqs. (2) and (3) and these conditions, we obtain the following relations:

$$\mu_O = \mu_{O_2-\mathrm{mol}} + \lambda \Delta H^{\mathrm{ZnO}}. \tag{4}$$

The chemical potential of europium oxide can be written as

$$\mu_{\mathrm{Eu_2}O_3} = \Delta H^{\mathrm{Eu_2}O_3} + 2\mu_{\mathrm{Eu\text{-}bulk}} + 3\mu_{\mathrm{O_2-mol}}, \tag{5}$$

where $\Delta H^{\mathrm{Eu_2}O_3}$ is the enthalpy of formation of europium oxide and $\mu_{\mathrm{Eu-bulk}}$ and $\mu_{\mathrm{O_2-mol}}$ are the europium bulk and oxygen molecule chemical potentials, respectively. This results in

$$\mu_{\mathrm{Eu}} \leqslant \tfrac{1}{2}\Delta H^{\mathrm{Eu_2}O_3} + \mu_{\mathrm{Eu\ bulk}} - \tfrac{3}{2}\lambda \Delta H^{\mathrm{ZnO}}. \tag{6}$$

Here, $\lambda = 0$ for oxygen rich and $\lambda = 1$ for oxygen poor conditions.

B. Electronic structure

The many-body methodology that is underlying the GW approximation goes back to pioneering work by Kadanoff and Baym [33,34] and Hedin [28]. In GW-based approximations, the screening of the Coulomb interaction, that enters the nonlocal self-energy operator, is calculated microscopically. This description of the screened potential W is a main advantage of many-body methods over other approaches, like hybrid functional DFT, where screening is only included phenomenologically.

The single-shot G_0W_0 approximation starting from GGA calculations often yields too small band gaps. It was suggested [31,35] that partially or fully self-consistent schemes, in which either Green's function G (GW_0) or both the Green's function and the dielectric matrix (GW) are updated can improve the agreement with experiments. We should mention that the implementation of self-consistent GW or GW_0 in VASP has the shortcoming, that only calculations that maintain a quasiparticle picture are possible, i.e., satellite peaks can not be accounted for. Even though this means that these are technically not "full" GW_0 calculations, we will for simplicity adopt the notation to call them GW and GW_0 in the following. For detailed information on the implementation, we refer the reader to Refs. [31,36–40].

III. RESULTS

A. Thermodynamic properties

It is in principle possible to calculate GW total energies by using the Galitskii-Migdal formula [41]. In Ref. [42] it was found that for the electron gas, the total energies can be well described using GW schemes. Alternative approaches to tackle the formation energy in connection with GW methods have been proposed [43,44]. In VASP, formation energies at GW level is not readily possible. Therefore we have decided to calculate the formation energies at GGA level. This can be justified taking into account that the GGA calculations are used as starting point for more accurate calculations using the GW method. We would like to mention that we have performed PBE0 calculations for some defects and we note that the location of Eu-f states are strongly dependent on the amount of HF included in the functional.

For europium oxide, the formation enthalpy is calculated to be $\Delta H^f(\mathrm{Eu_2O_3}) = -14.43$ eV compared with the experimental value of -16.51 eV [45]. For zinc oxide, the formation enthalpy is $\Delta H^f(\mathrm{ZnO}) = -2.90$ eV, which is in good agreement with other GGA values [46] and even GGA+U calculations [22]. This discrepancy is probably due to the wrong description of the oxygen molecule, as has been discussed in Ref. [47]. Using these values, we can obtain the binding energy of the defect complexes, which are defined as

$$\mathrm{E_{binding}} = \mathrm{E_f^{complex}} - \sum_{\mathrm{i}} \mathrm{E_f^{isolated}}, \tag{7}$$

where $\mathrm{E_f^{complex}}$ is the formation energy of the defects and $\mathrm{E_f^{isolated}}$ is the formation energy of isolated defects calculated according to Eq. (1). The calculated values are shown in Table I and a negative value means that the complex is stable. Calculations for intrinsic defects can reproduce well previous calculations reported using local functionals [46,48,49]. Neutral oxygen vacancies have a low-formation energy under oxygen poor conditions. On the other hand, zinc vacancies can be formed under Zn-poor preparation conditions. Oxygen and zinc interstitials, as expected, have high formation energies, due to their size [49]. For Eu-doped ZnO at cation site, we obtain a formation energy of 2.42 eV under O-rich conditions. Incorporation of Eu at interstitial positions is

TABLE I. Formation energies E_f and binding energies E_b for neutral intrinsic defects and defect complexes in ZnO.

	E_f (eV)		E_b (eV)	
Defect	O-rich	O-poor	O-rich	O-poor
Eu_{Zn}	2.42	7.44		
$O_{i(split)}$	2.58	5.48		
$O_{i(oct)}$	3.38	6.28		
V_O	3.20	0.30		
V_{Zn}	1.37	4.27		
Zn_{int}	6.68	3.78		
Eu_{Zn} + Oi(split)	4.52	14.67	−0.48	1.75
Eu_{Zn} + Oi(oct)	4.4	14.55	−1.40	0.83
$Eu_{Zn} + V_O$	6.1	10.45	0.48	2.70
$Eu_{Zn} + V_{Zn}$	10.9	13.80	7.11	2.09
$Eu_{Zn} + Zn_{int}$	9.88	12.78	0.79	1.56

highly unfavorable, due to the strain Eu causes in the ZnO, leading to a strongly distorted lattice. Similar results have been reported in Ref. [50]. Complex formation with zinc and oxygen vacancies and zinc interstitials have a much higher formation energy. This can be understood by considering size effects, which causes a large strain in the lattice. As the defect complexes are formed in experiments under extreme nonequilibrium conditions (like, e.g., ion implantation), we find it more appropriate to report the binding energies of the defect complexes and hence their stability against dissociation.

As we can see, the most stable neutral defect is under O-rich conditions the Eu-O_i(o) complex. It is interesting to point out that the formation of neutral oxygen defects at interstitial sites in pure ZnO has a high formation energy under thermodynamic equilibrium. However, as has been shown in Ref. [49] the diffusion barrier for this kind of defect is relatively low (around 0.2 eV). Therefore once this defect is formed under ion implantation (nonequilibrium conditions), it can rapidly diffuse in the material and form complexes with europium atoms. This may explain why the complex Eu-O_i(o) is so stable in ZnO.

Now let us discuss the charged complexes. In Fig. 1, we show the formation energies of several Eu complexes as a function of the Fermi energy at O-rich and Zn-rich conditions. The top of the valence band $\mathbf{E_v}$ for all defects calculations was aligned with the top of the valence band of the host ZnO using the averaged electrostatic potential as described in Ref. [32]. We see that the most stable structure at O-rich conditions is a complex of Eu-$O_{i(oct)}$ in the −1 charge state. Although this is the thermodynamically most stable defect, followed by Eu subst and Eu − V_O(−1), we argue that the fact that the neutral Eu-$O_{i(oct)}$ corresponds to the experimental f-f transition is very appealing. Obviously, we cannot rule out the co-existence of these other defects during the preparation conditions. Further calculations are needed to clarify whether these defects also have transitions in the experimentally observed region. On the other hand at Zn-rich conditions, the defect Eu-subst is the most stable one for $E_F - E_v$ between 0 and 0.6. For values larger than that, the defect Eu-V_O in the −1 charge state is the most stable one. It is important to note that under Zn-rich conditions all defects have a very high formation energy, which is an indication that they are unlikely to form at these conditions.

B. Electronic properties

Because GW calculations can be performed using different approximations, the results for the theoretical band gap of ZnO

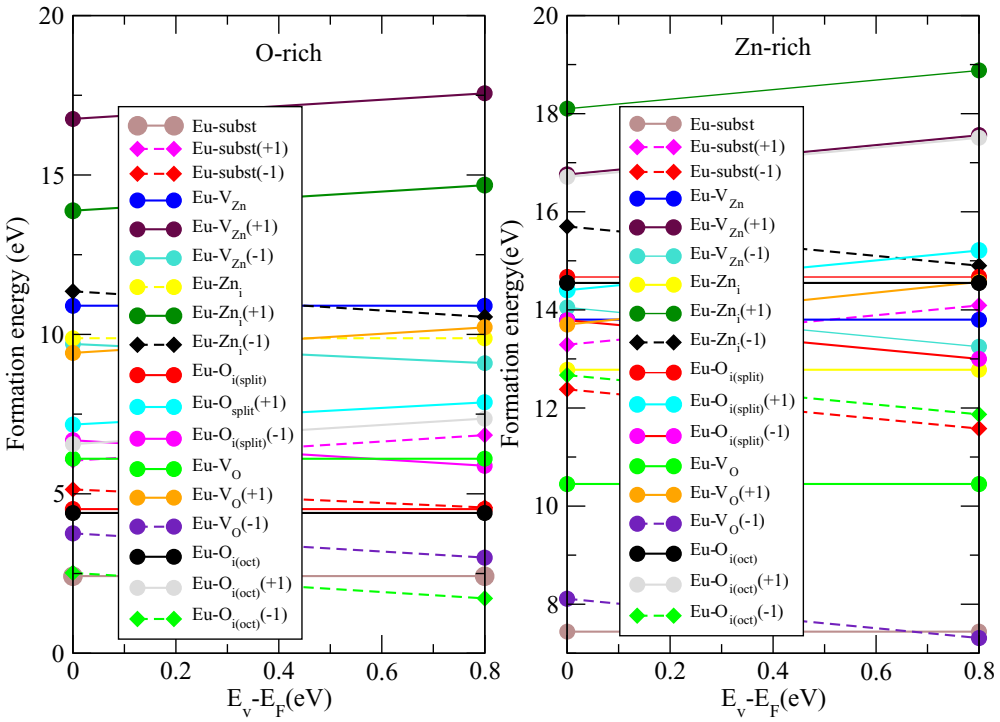

FIG. 1. Formation energies of several Eu complexes as a function of the Fermi energy (a) O-rich and (b) Zn-rich conditions.

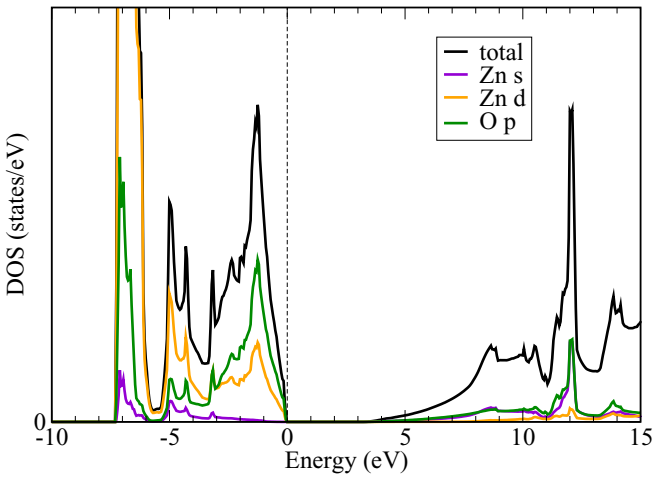

FIG. 2. Density of states of bulk ZnO calculated in the PBE + GW_0 approximation. The vertical line denotes the highest occupied state.

has been under debate. Parameters controlling the calculations include the number of bands [51–53], the exchange-correlation potential for the starting wave function [22] as well as the use of approximate models for the screening, like plasmon pole approximations [51].

Depending on the starting functional and the details of the calculation, values between 2.1 and 3.6 eV are obtained for G_0W_0 [24,31,39,40,51–54], between 2.54–3.6 for GW_0 [24,39,54–56] and between 3.2–4.3 for GW [24,37].

We start by validating the GW_0 method for bulk ZnO. For this purpose we consider a four-atom wurzite ZnO unit cell and employ a $8 \times 8 \times 8$ **k**-point sampling with an energy cutoff of 500 eV. The resulting band gaps and energetic positions of the Zn-3d states (with respect to the valence-band maximum set at zero) for several levels of GW calculations are (a) PBE: 0.8 and −5.1 eV, (b) PBE0: 3.2 and −7.3 eV, (c) HSE06: 2.5 and −7.1 eV, (d) PBE + GW: 4.3 and −7.2 eV, and (e) PBE + GW_0: 3.3 and −7.0 eV.

For the GW_0 calculation, a cutoff of 200 eV for the response functions χ, as well as 1024 bands have been employed. It has been shown that a large number of bands is necessary to obtain properly converged results in earlier one-shot G_0W_0 calculations [51–53]. We speculate that the deviations to Ref. [54] are due to the rather low number of bands in that publication. The results are shown in Fig. 2. We find a band gap of 3.3 eV in reasonable agreement with the experimental value of 3.44 eV [57], as well as with other all-electron GW_0 calculations [53,55]. It should be pointed out that recently norm conserving pseudopotentials were introduced in VASP to improve GW calculations [53]. However, as shown in Ref. [53], we expect these to only lead to minor modifications of the band structure of up to 0.2 eV, not changing the main conclusions of this work. It should be noted that that use of GW-based methods has been able to predict the positions of lanthanide f states in NiO [58] and CeO_2 [25].

The center of the Zn-d orbitals is localted at −7 eV, in agreement with previous GW_0-calculations for ZnO [31,55,59]. We want to point out, that a fully selfconsistent GW calculation results in a much too high quasiparticle gap of 4.2 eV. Again

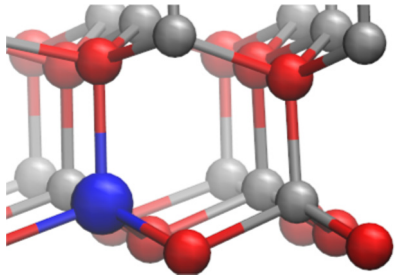

FIG. 3. Atomic structure around the europium impurity calculated within GGA for substitutional europium in ZnO. Blue, red, and grey spheres are Eu, O, and Zn atoms, respectively.

this agrees well with recent all-electron calculations that find a quasiparticle gap of 4.3 [55].

From here on we show only results for GW_0 calculations. It has been shown that the position of defect states is not strongly influenced by the number of empty bands and the response function cutoff [24]. The relaxed geometry of Eu at a zinc lattice position without the presence of intrinsic defects is shown in Fig. 3. The europium distance to nearest oxygen atoms are 2.23 and 2.27 Å for in-plane and **c** directions, respectively. These values are slightly larger than the Zn-O bond lengths in pure ZnO. This means that if Eu is incorporated at a Zn lattice position, it should not disturb the lattice significantly. We would like to point out that in the supercell GW_0 calculations, the ZnO band gap is slightly to large, around 3.6–3.9 eV. We attribute this to the reduced k-point sampling in the supercell calculation. We also several tests with scGW_0 calculations, to also investigate the influence of a selfconsistent update of also the wave-functions. In these tests, we find that quasiparticle energies are only changed by up to 0.1–0.2 eV between scGW_0 and GW_0 calculations, supporting the use of the GW_0 approximation in the following.

In Fig. 4, the GW_0 electronic density of states of substitutionally incorporated Eu in this geometry is shown. The Eu-f states lie within the band gap, around 2 eV above the VBM

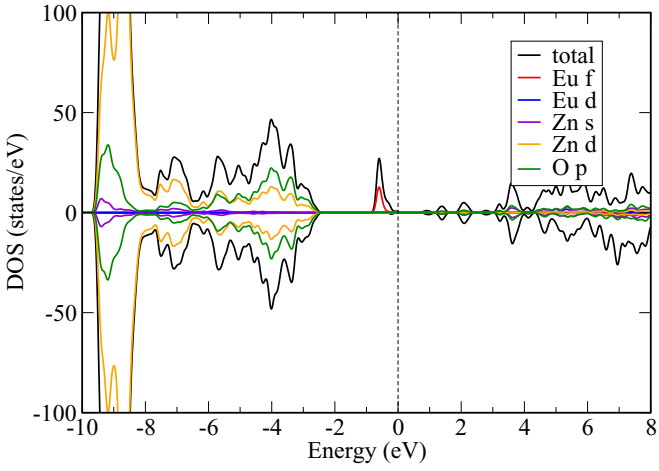

FIG. 4. Total and projected density of states for Eu at Zn site in ZnO calculated within the PBE0+GW_0 approximation. The vertical dashed line denotes the highest occupied state. Positive (negative) values of the DOS denote spin up (down).

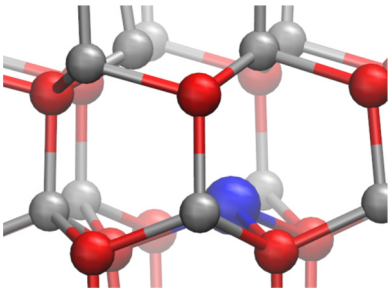

FIG. 5. Atomic structure around the Eu-V_O complex calculated within GGA. Blue, red, and gray spheres are Eu, O, and Zn atoms, respectively.

(valence-band maximum), hybridize weakly with the Zn-s and O-p states. As expected for substitutional Eu at a Zn lattice position, Eu has a formal charge closer to 2+. The f spin-up orbitals are fully occupied, giving a total magnetic moment of $7\mu_B$. Furthermore, the Eu d states lie deep in the conduction band of ZnO, ≈2.5 eV above the CBM, leading to an energetic difference to the Eu f states of over 3 eV. Therefore our results explain why the $4f^7 - 4f^6/5d^1$ optical transition at 530 nm (≈2.3 eV) that is often observed additionally to the intra-f transitions for Eu incorporation into other host materials can not be found experimentally in Eu-doped ZnO [5,11].

A possible way to modify the oxidation state of Eu in the ZnO lattice is therefore a change of its environment. It is known that during ion implantation intrinsic defects are likely to form [5,17]. We therefore investigated Eu-doped ZnO in the presence of nearby oxygen and zinc vacancies as well as zinc and oxygen interstitials. In the presence of a neutral oxygen vacancy the Eu-O distances for neighboring oxygen atoms remain almost unchanged, compared to the case without vacancy, and increase slightly to 2.24 Å. The geometry is shown in Fig. 5. The Eu-Zn distance is 3.27 Å and relaxation of farther neighbors is insignificant.

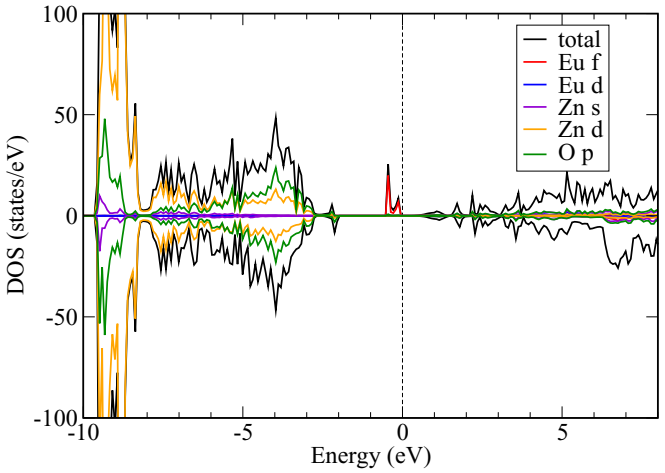

FIG. 6. Total and projected density of states for Eu incorporated at Zn position in ZnO next to a oxygen vacancy calculated within the PBE0+GW_0 approximation. The vertical line denotes the highest occupied state. Positive (negative) values of the DOS denote spin up (down).

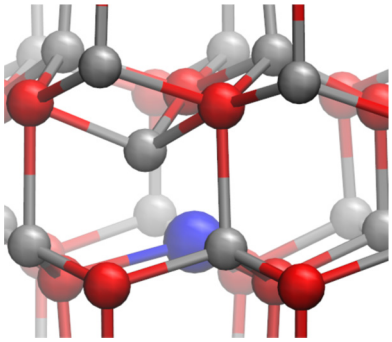

FIG. 7. Atomic structure around the Eu-Zn_i complex calculated within GGA. Blue, red, and gray spheres are Eu, O, and Zn atoms, respectively.

The electronic structure for this system is shown in Fig. 6. The states due to the oxygen vacancy lie 1 eV above the VBM. This is in good agreement with calculations for pure ZnO (see, e.g., Refs. [23,46,48]). The Eu f states are located now at 2.5 eV above the VBM. Moreover, we observe a small splitting of the Eu-f states as well as a small hybridization with the Eu-d and O-p states. The splitting is caused by a shift of one of the seven Eu-f states that we assume to be induced by changes in the local environment that affect the interaction matrix elements and therefore the charge distribution around the impurity.

Our GW_0 results are in strong contrast to the findings of Ref. [18], where the Eu-f states are energetically located directly above the V_O states. We attribute this discrepancy to the choice of the GGA functional in Ref. [18], predicting a much too narrow band gap. On the other hand, the presence of the V_O does not significantly change the formal charge around the Eu atom. Moreover, the positions of the Eu-f spin down and Eu d-states remain practically unchanged. Again this defects cannot explain the experimental observed f-f transition in ZnO.

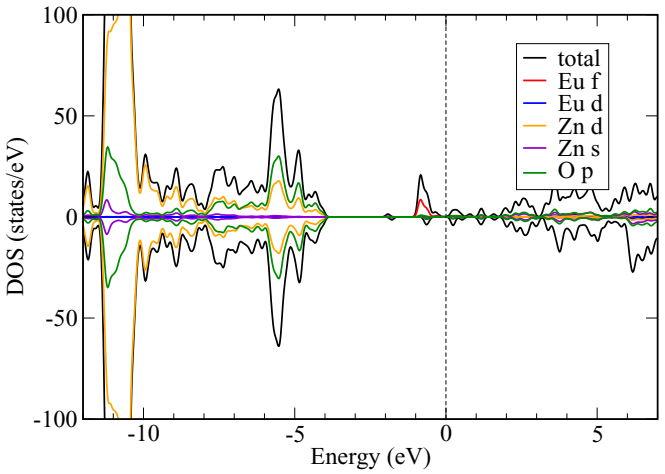

FIG. 8. Density of states of Eu-doped ZnO in the presence of a nearby zinc interstitial calculated within the PBE0+GW_0 approximation. The vertical line denotes the highest occupied state. Positive (negative) values are the spin up (down) components.

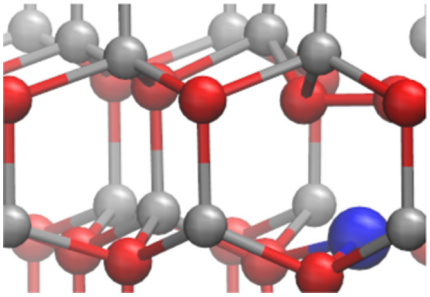

FIG. 9. Atomic structure around the Eu-O_{int}^{split} complex calculated within GGA. Blue, red, and gray spheres are Eu, O, and Zn atoms, respectively.

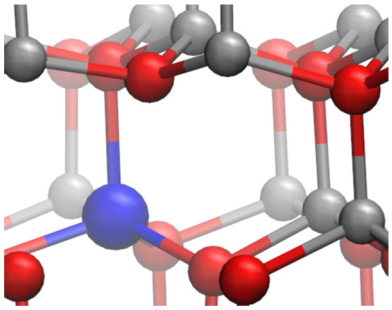

FIG. 11. Atomic structure around the Eu-V_{Zn} complex within GGA. Blue, red, and gray spheres are Eu, O, and Zn atoms, respectively.

The relaxed geometry of the Eu+Zn_i defect is shown in Fig. 7. The bond lengths between the Eu atom and the nearest oxygen atoms are 2.19, 2.19, and 2.24 Å in the in-plane direction, and 2.41 Å in the **c** direction. This is because Eu atom relaxes away from the Zn atom. The Eu-Zn distance is 2.72 Å, while the distances to Zn second neighbors are 3.29 Å.

The electronic structure of this system is shown in Fig. 8. The location of the Eu-f states lies close to the conduction band minimum (CBM), around 2.9 eV above the VBM. We can infer a weak hybridization with both Zn-s and Zn-d states of the Zn interstitial atom. Similarly, a very small hybridization with the O-p states is found. Here, the formal charge of the Eu atom remains close to 2+ with the spin-up f states occupied.

For the oxygen interstitial plus Eu defect, we have considered two geometries. The first consists of an Eu atom at substitutional Zn site next to an oxygen interstitial in dumbbell configuration [60]. This configuration is shown in Fig. 9. In this case, the lattice ralaxations are more pronounced. The Eu atom is shifted away from the interstitial complex, decreasing the Eu-O bond lengths to 2.21 Å. The Eu-Zn distance is also slightly increased to 3.29 Å and the distances to the oxygen atoms of the interstitial are 2.31 and 2.33 Å, respectively.

The electronic structure is presented in Fig. 10. We observe a splitting of the Eu-f states that we attribute to a combination of the changed symmetry in the local environment. This affects both the interaction matrix elements as well as their screening, so that different Eu states are influences differently. While six of the Eu-f are located closer to the VBM, the remaining occupied Eu-f state lies about 1 eV higher in energy. We find contributions to the localized states from both O_{int-p} and O_{host} states. However, also in this case, the Eu atom possesses a formal charge of 2+ with all Eu-f spin-up states fully occupied. The oxygen interstitial atom possesses a magnetic moment of $0\mu_B$, a further confirmation, that no electron is transferred from the Eu atom to the oxygen site.

The geometry of Eu-doped ZnO in the presence of a neutral Zn vacancy (V_{Zn}) is shown in Fig. 11. The Eu atom shifts towards the vacancy, increasing the in-plane Zn-Eu distance to 3.49 and 3.40Å in comparison to 3.3 Å that would correspond to Eu exactly on Zn lattice position. Consequently, the in-plane Eu-O distances also change, asymmetrically, to 2.09, 2.19, and 2.24 Å, respectively. Along the **c**-direction the Eu-O distance is 2.22 Å. The corresponding electronic structure is shown in Fig. 12. We find no occupied Eu-f states in the band gap. These states lie within the VB, close to the O-p states and hybridize

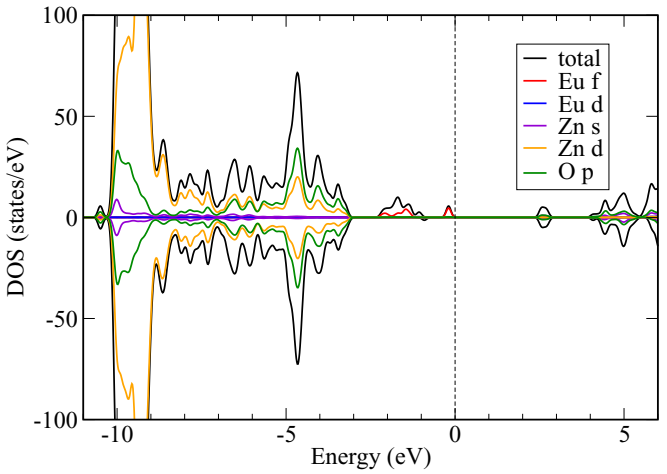

FIG. 10. Density of states of Eu-doped ZnO in the presence of a nearby split oxygen interstitial calculated within the PBE0+GW_0 approximation. The vertical line denotes the highest occupied state. Positive (negative) values are the spin up (down) components.

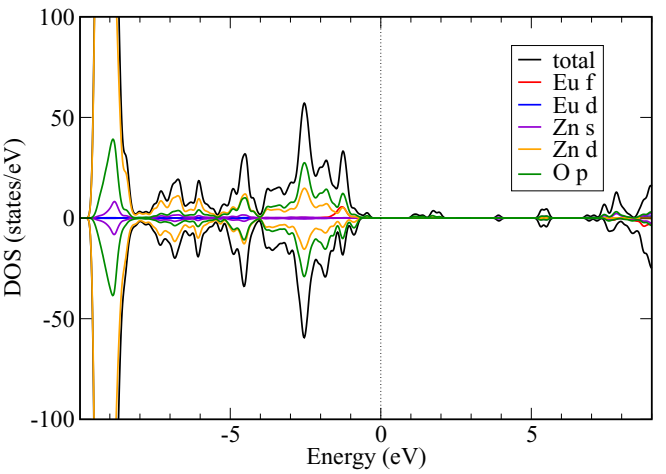

FIG. 12. Density of states of Eu-doped ZnO in the presence of a nearby zinc vacancy calculated within the PBE0+GW_0 approximation. The vertical line denotes the highest occupied state. Positive (negative) values are the spin-up (down) components.

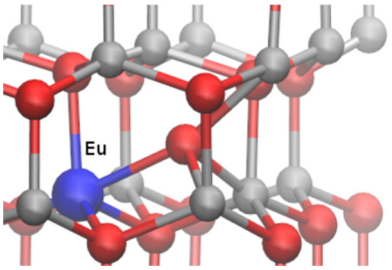

FIG. 13. Atomic structure around the Eu+O_{int}^{oct} complex within GGA. Blue, red, and gray spheres are Eu, O, and Zn atoms, respectively.

both with with O-p and Zn-d states. The local projected moment on the V_{Zn} site is $1\mu_B$, which is aligned antiparallel to the magnetic moment on the Eu which is $6\mu_B$. However, the fact that the Eu-f states are energetically located inside the VB and the unoccupied Eu-f state is energetically located at 2 eV above the VBM, does not fit with experimentally observed transition.

The other defect complex including an oxygen interstitial consists of an oxygen at a octahedral interstitial site next to an Eu at Zn lattice position. The corresponding atomic structure is shown in Fig. 13. We find much more pronounced lattice relaxations in this case, also involving second nearest neighbors. The Eu-Zn distance is 3.2 Å, while the Eu-O bond lengths are 2.2 Å to the oxygen atoms in the basal plane and 2.25 Å to the oxygen along the c direction. The distance between the Eu atom and the oxygen interstitial is 2.24 Å. This can be explained by looking at the coordination Eu adopts. The Eu-O distance to the nearest neighbors is very similar to Eu_2O_3, which possess a coordination number of 6 ± 1 and a radial distance of 2.33 $\pm$0.015 Å according to Ref. [61].

The corresponding electronic structure is shown in Fig. 14. We find the occupied Eu f-states are located in the band gap, with the Eu-f orbitals being occupied with six electrons. The

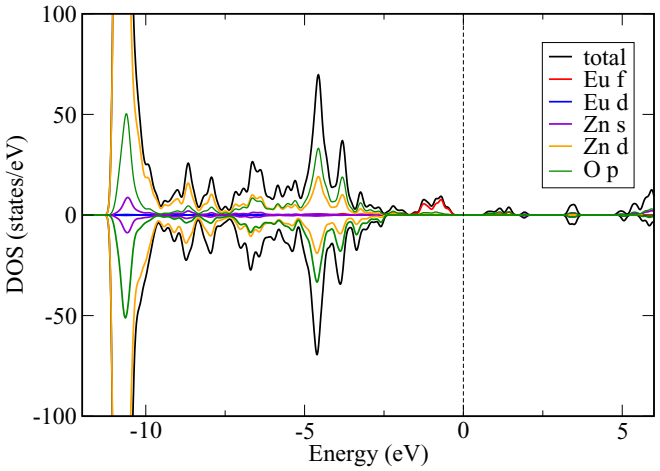

FIG. 14. Density of states of Eu-doped ZnO in the presence of a nearby octahedral oxygen interstitial calculated within the PBE0+GW_0 approximation. The vertical dashed line denotes the highest occupied state. Positive (negative) values are the spin up (down) components.

TABLE II. Relative position of Eu-f states for the investigated complexes with respect to the top of the valence band of ZnO. The position of the Eu-f states were taken approximately in the middle of the f bands. All values are given in eV.

Complex	$E_{VB} - E_f$
Eu_{Zn}	2.8
Eu_{Zn} + Oi(split)	1.5/3.2
Eu_{Zn} + Oi(oct)	2.5
$Eu_{Zn} + V_O$	2.5/3.2
$Eu_{Zn} + V_{Zn}$	1.0
$Eu_{Zn} + Zn_{int}$	3.8

occupied and unoccupied states are located at -0.7 and 1.3 eV, respectively. We find a small hybridization with O-$p_{i(oct)}$ and O-$p_{(host)}$. The total magnetic moment of the complex is $5\mu_B$, determined by a magnetic moment of $6\mu_B$ spin up at the europium aligned anti-parallel to the magnetic moment of $1\mu_B$ at the oxygen interstitial atom. Therefore we suggest that the intra-4f luminescence of the ZnO:Eu samples is most likely due to Eu_{Zn}+O_i^{oct} complexes. We have also explored the mechanism for optical activation of Eu in ZnO reported in Ref. [15], where substitutional hydrogen at Zn lattice position next to an europium atom is suggested. However, this configuration does not change the formal charge of Eu.

In order to summarize the results discussed above, we show the position of the defect levels with respect to the band edges of ZnO. The results are shown in Table II. We show the relative position of Eu-f states for the complexes with respect to the top of the valence band of ZnO. The position of the Eu-f states were taken approximately in the middle of the f bands, since we cannot describe correctly with DFT the multiplets of the f orbitals.

IV. CONCLUSIONS

In conclusion, we have investigated Eu-doped ZnO using DFT and the many-body GW technique within the GW_0 approximation. We find that the position and formal charge of the Eu-f states is strongly dependent on the environment around the Eu atom. We conclude that the optical activity of Eu in ZnO is most likely due to Eu+O_i^{oct} defect complexes, possibly either in a neutral or -1 charge state or in the presence of both. Finally, we believe our results can open the pathway for a better understanding of these complexes in zinc oxide.

ACKNOWLEDGMENTS

We acknowledge fruitful discussions with R. Röder, C. Ronning, and H. Chacham and financial support from the Deutsche Forschungsgemeinschaft under the programm FOR1616. A. L. da Rosa would like to thank financial support from CNPq under the program "Science without Borders." We also thank HLRN (Hannover/Berlin) for computational resources.

[1] S. Geburt, M. Lorke, A. L. da Rosa, T. Frauenheim, R. Röder, T. Voss, U. Kaiser, W. Heimbrodt, and C. Ronning, Nano Lett. **14**, 4523 (2014).

[2] A. Ishizumi, Y. Taguchi, A. Yamamoto, and Y. Kanemitsu, Thin Solid Films **486**, 50 (2005).

[3] M. Peres, A. Cruz, S. Pereira, M. Correia, M. Soares, A. Neves, M. Carmo, T. Monteiro, A. Pereira, M. Martins *et al.*, Appl. Phys. A **88**, 129 (2007).

[4] C. Pan, C. Chen, J. Chen, P. Huang, G. Chi, C. Chang, F. Ren, and S. Pearton, Appl. Surf. Sci. **256**, 187 (2009).

[5] C. Ronning, C. Borschel, S. Geburt, R. Niepelt, S. Mller, D. Stichtenoth, J. P. Richters, A. Dev, T. Voss, L. Chen *et al.*, Phys. Status Solidi B **247**, 2329 (2010).

[6] U. Wahl, E. Rita, J. G. Correia, E. Alves, J. P. Araújo, and T. I. Collaboration, Appl. Phys. Lett. **82**, 1173 (2003).

[7] U. Wahl, J. G. Correia, E. Rita, E. Alves, J. C. S. B. D. Vries, V. Matias, A. Vantomme, and T. I. Collaboration, Hyperfine Interact. **159**, 363 (2004).

[8] Y.-P. Du, Y.-W. Zhang, L.-D. Sun, and C.-H. Yan, J. Phys. Chem. C **112**, 12234 (2008).

[9] S. Ji, L. Yin, G. Liu, L. Zhang, and C. Ye, J. Phys. Chem. C **113**, 16439 (2009).

[10] K. Ebisawa, T. Okuno, and K. Abe, Jpn. J. Appl. Phys. **47**, 7236 (2008).

[11] J. Petersen, C. Brimont, M. Gallart, G. Schmerber, P. Gilliot, C. Ulhaq-Bouillet, J.-L. Rehspringer, S. Colis, C. Becker, A. Slaoui *et al.*, Jpn. J. Appl. Phys. **107**, 123522 (2010).

[12] Q. Q. Dai, L. Luo, F. Y. Huang, D. P. Xiong, X. Tang, and J. Chen, Mater. Sci. Forum **687**, 667 (2011).

[13] T. Tsuji, Y. Terai, M. H. B. Kamarudin, K. Yoshida, and Y. Fujiwara, J. Lumin. **132**, 3125 (2012).

[14] M. Mezdrogina, M. Eremenko, S. Golubenko, and S. Razumov, Phys. Solid State **54**, 1235 (2012).

[15] H. Akazawa and H. Shinojima, J. Appl. Phys. **114**, 153502 (2013).

[16] L. Yang, J. Dong, Y. She, Z. Jiang, L. Zhang, and H. Yu, Appl. Phys. Lett. **104**, 033109 (2014).

[17] D. Wang, G. Xing, M. Gao, L. Yang, J. Yang, and T. Wu, J. Phys. Chem. C **115**, 22729 (2011).

[18] M. Assadi, Y. Zhang, R.-K. Zheng, S. Ringer, and S. Li, Nanoscale Res. Lett. **6**, 357 (2011).

[19] L. Chen, H. Hu, and Z. Xiong, Appl. Phys. Frontier **1**, 22 (2013).

[20] S. Lany and A. Zunger, Phys. Rev. B **78**, 235104 (2008).

[21] S. Lany and A. Zunger, Modell. Simul. Mater. Sci. Eng. **17**, 084002 (2009).

[22] S. Lany and A. Zunger, Phys. Rev. B **81**, 113201 (2010).

[23] A. Janotti and C. G. V. de Walle, Rep. Prog. Phys. **72**, 126501 (2009).

[24] I. A. Sarsari, C. D. Pemmaraju, H. Salamati, and S. Sanvito, Phys. Rev. B **87**, 245118 (2013).

[25] H. Jiang, R. I. Gomez-Abal, P. Rinke, and M. Scheffler, Phys. Rev. Lett. **102**, 126403 (2009).

[26] P. Hohenberg and W. Kohn, Phys. Rev. **136**, B864 (1964).

[27] W. Kohn and L. J. Sham, Phys. Rev. **140**, A1133 (1965).

[28] L. Hedin, Phys. Rev. **139**, A796 (1965).

[29] P. E. Blöchl, Phys. Rev. B **50**, 17953 (1994).

[30] G. Kresse and D. Joubert, Phys. Rev. B **59**, 1758 (1999).

[31] M. Shishkin, M. Marsman, and G. Kresse, Phys. Rev. Lett. **99**, 246403 (2007).

[32] C. van de Walle and J. Neugebauer, J. Appl. Phys. **95**, 3851 (2004).

[33] G. Baym and L. Kadanoff, Phys. Rev. **124**, 287 (1961).

[34] G. Baym, Phys. Rev. **127**, 1391 (1962).

[35] U. von Barth and B. Holm, Phys. Rev. B **54**, 8411 (1996).

[36] P. Rinke, A. Qteish, J. Neugebauer, C. Freysoldt, and M. Scheffler, New J. Phys. **7**, 126 (2005).

[37] M. Usuda, N. Hamada, T. Kotani, and M. van Schilfgaarde, Phys. Rev. B **66**, 125101 (2002).

[38] J. A. Berger, L. Reining, and F. Sottile, Phys. Rev. B **85**, 085126 (2012).

[39] F. Hüser, T. Olsen, and K. S. Thygesen, Phys. Rev. B **87**, 235132 (2013).

[40] A. Malashevich, M. Jain, and S. G. Louie, Phys. Rev. B **89**, 075205 (2014).

[41] A. L. Fetter and J. D. Walecka, *Quantum Theory of Many-Particle Systems*, 2nd ed. (Dover, Mineola, New York, 2003).

[42] B. Holm, Phys. Rev. Lett. **83**, 788 (1999).

[43] P. Rinke, A. Janotti, M. Scheffler, and C. G. Van de Walle, Phys. Rev. Lett. **102**, 026402 (2009).

[44] G. Samsonidze, M. Jain, J. Deslippe, M. L. Cohen, and S. G. Louie, Phys. Rev. Lett. **107**, 186404 (2011).

[45] Handbook of Chemistry and Physics Online (2014), http://www.hbcpnetbase.com/.

[46] F. Oba, M. Choi, A. Togo, and I. Tanaka, Sci. Technol. Adv. Mater. **12**, 034302 (2011).

[47] J. P. Perdew, K. Burke, and M. Ernzerhof, Phys. Rev. Lett. **77**, 3865 (1996).

[48] F. Oba, M. Choi, A. Togo, A. Seko, and I. Tanaka, J. Phys.: Condens. Matter **22**, 384211 (2010).

[49] A. Janotti and C. G. Van de Walle, Phys. Rev. B **76**, 165202 (2007).

[50] V. Ney, S. Ye, T. Kammermeier, K. Ollefs, F. Wilhelm, A. Rogalev, S. Lebègue, A. L. da Rosa, and A. Ney, Phys. Rev. B **85**, 235203 (2012).

[51] B.-C. Shih, Y. Xue, P. Zhang, M. L. Cohen, and S. G. Louie, Phys. Rev. Lett. **105**, 146401 (2010).

[52] C. Friedrich, M. C. Müller, and S. Blügel, Phys. Rev. B **83**, 081101 (2011).

[53] J. Klimeš, M. Kaltak, and G. Kresse, Phys. Rev. B **90**, 075125 (2014).

[54] Y. Kang, G. Kang, H.-H. Nahm, S.-H. Cho, Y. S. Park, and S. Han, Phys. Rev. B **89**, 165130 (2014).

[55] C. Friedrich (private communication).

[56] G. Petretto and F. Bruneval, Phys. Rev. Appl. **1**, 024005 (2014).

[57] *Semiconductors – Basic Data*, edited by O. Madelung, 2nd ed. (Springer, Berlin, 1996).

[58] V. I. Anisimov, F. Aryasetiawan, and A. Lichtenstein, J. Phys.: Condens. Matter **9**, 767 (1997).

[59] F. Fuchs, J. Furthmüller, F. Bechstedt, M. Shishkin, and G. Kresse, Phys. Rev. B **76**, 115109 (2007).

[60] P. Erhart, A. Klein, and K. Albe, Phys. Rev. B **72**, 085213 (2005).

[61] G. E. Fryxell, H. Wu, Y. Lin, W. J. Shaw, J. C. Birnbaum, J. C. Linehan, Z. Nie, K. Kemner, and S. Kelly, J. Mater. Chem. **14**, 3356 (2004).